

Demanded Power Point Tracking of PV Power Plants without Battery Energy Storage

Stephan Kusche, Horst Schulte¹

¹Control Engineering Group, Department of Engineering I
University of Applied Sciences Berlin (HTW), Germany
E-Mail: kusche,schulte@htw-berlin.de

Abstract

Future electrical power systems operating up to 100-percent with regenerative energy sources (RES) will need dynamically controllable power plants [1]. The variables to be controlled in power systems are voltage and frequency of the grid. Thereby, the frequency in the grid is changed via the supplied power of the power plants. Until recently, regenerative energy systems have fed as much power as possible into the grid with the objective of optimizing the power by means of maximum power point (MPP) tracking [2]. Therefore, they contribute to grid stability only to a very limited amount. To change the paradigm, control methods like active power tracking control of wind turbines (WT) [3] and photovoltaic (PV) power plants with battery storage have been developed in recent years. However, it is also necessary that PV systems without storage can quickly reduce the power to be supplied. In this paper, a model-based demanded power point (DPP) tracking controller based on Takagi-Sugeno modeling and LMI synthesis is presented. It has the advantage to perform in a wide nonlinear operating range with guaranteed performance, independent of external disturbances such as changes in the irradiation and PV cell temperature.

DOI: 10.58895/ksp/1000138532-11 erschienen in:

Proceedings - 31. Workshop Computational Intelligence : Berlin, 25. - 26. November 2021

DOI: 10.58895/ksp/1000138532 | <https://www.ksp.kit.edu/site/books/m/10.58895/ksp/1000138532/>

1 Introduction

Currently the major part of the electrical energy is produced by classical synchronous machines. They have the inherent ability to stabilize the electrical grid due to their inertia. Droops in voltage and grid frequency have to overcome this inertia first in order to make any changes to these quantities.

Until 2020, the photovoltaic electricity share was about 8.7% and 3.9% in Germany and EU28, respectively [4]. In the past, this small share allows renewable energy sources (RES) to simply feed their complete available power into the grid without paying attention to the grid stability. Nevertheless the share of renewable electrical energy is deliberately rising. With higher share, the grid stability becomes a serious issue that has to be addressed by new control concepts. One possible approach is to engineer renewable energy sources in a way that they act like a conventional power plant with an inherent inertia, see e.g. [5, 6]. Optimization can be achieved by forming an intelligent compound of these power plants, called dynamic virtual power plant (DVPP) [7]. Participants to the digital virtual power plant need to be able to meet minimum requirements like controllable power generation under varying conditions and they need to supply a proper communication interface.

A usual model scheme for a PV power plant is shown in Figure 1. The primary converter can be identified at the DCDC-converter by the converter model and the converter controller. Its task is to regulate the voltage of the PV cell v_{pv} and to feed the electrical power into the DC link. The MPP respectively DPP controller can be interpreted as part of the power plant controller. The secondary converter can be located at the grid connection. Its task is the power conversion at the grid level and it connects to the PCC. In the following, we will discuss the electrical model of the PV cell and the complete DCDC-converter.

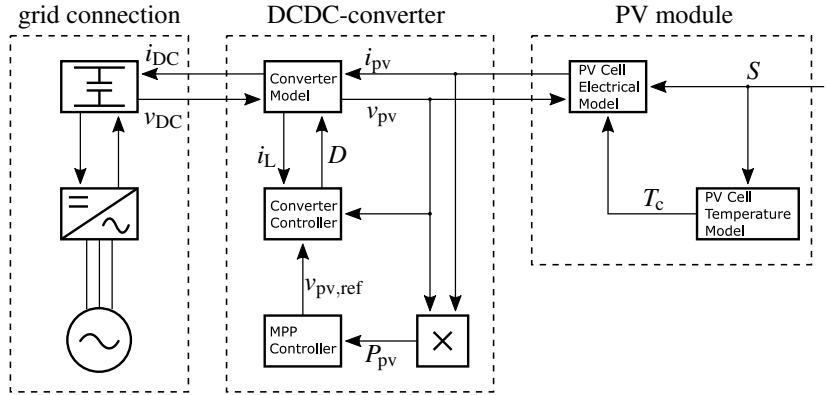


Figure 1: Signal paths for the PV power generator from the physical power source (irradiation S on the right hand side) to the electrical grid (in the left hand side).

2 Model of PV Module

The well known complete single diode model (cSDM) is shown in Figure 2 [8]. It consists of the ideal model of a photovoltaic cell (current source in parallel with a diode) completed by resistors in serial and parallel to accommodate losses. The diode I-V characteristic is described by the theory of Shockley [9]:

$$i_d = i_s \left[\exp \left(\frac{1}{A_n} \frac{v_d}{v_T} \right) - 1 \right], \quad v_T = \frac{k_B T_c}{q_e}. \quad (1)$$

where

$A_n \in [1, 2],$	ideality factor of the diode [1]
$i_d,$	diode current [A]
$i_s,$	diode reverse-bias saturation current [A]
$k_B,$	Boltzmann constant [$1.38 \cdot 10^{-23} \text{ J/K}$]
$q_e,$	elementary charge [$1.602 \cdot 10^{-19} \text{ C}$]
$T_c,$	absolute temperature of the p-n junction, cell temperature [K]
$v_d,$	voltage across the diode [V]
$v_T,$	thermal voltage [V]

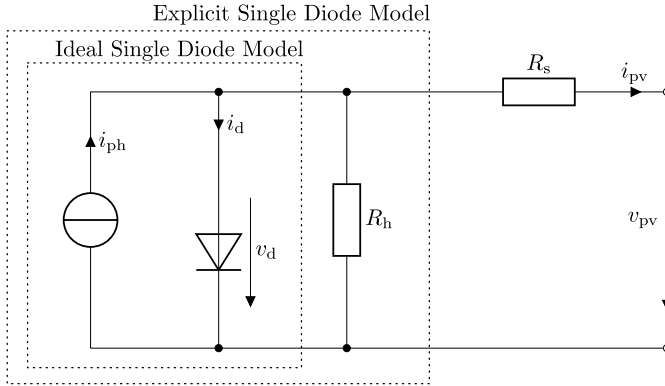


Figure 2: Complete Single Diode Model and simplifications thereupon.

Together with Kirchhoff's first circuit law $i_{pv} = i_{ph} - i_d - v_d/R_h$ and Kirchhoff's second circuit law $v_d = v_{pv} + R_s i_{pv}$ this gives the following relation between i_{pv} and v_{pv} :

$$i_{pv} = i_{ph} - i_s \left[\exp \left(\frac{v_{pv} + R_s i_{pv}}{v_T A_n} \right) - 1 \right] - \frac{v_{pv}}{R_h} - \frac{R_s}{R_h} i_{pv}. \quad (2)$$

where

$$\begin{cases} i_{ph}, & \text{photon current [A]} \\ i_{pv}, & \text{PV cell current [A]} \\ R_h, & \text{shunt resistance } [\Omega] \\ R_s, & \text{series resistance } [\Omega] \\ v_{pv}, & \text{PV cell voltage [V]} \end{cases}$$

2.1 Explicit Single Diode Model (eSDM)

The cSDM includes 5 fitting parameters: $(A_n, i_s, i_{ph}, R_h, R_s)$. In dependence on the amount and accuracy of the data provided by the manufacturer about the photo cells I-V-characteristic, it can be hard to identify all 5 parameters. Furthermore, (2) gives only an implicit function for the photon current. To

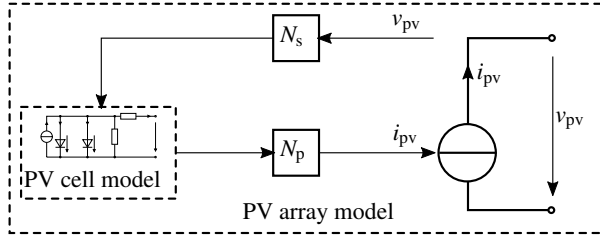


Figure 3: Aggregation of the PV array model from PV cell model.

obtain an explicit form, the cSDM is simplified by setting R_s to zero leading to the eSDM. The governing equation (2) becomes:

$$i_{pv} = i_{ph} - i_s \left[\exp \left(\frac{1}{A_n} \frac{v_{pv}}{v_T} \right) - 1 \right] - \frac{v_{pv}}{R_h} = f(v_{pv}). \quad (3)$$

For the open-circuit $i_{pv} = 0$, it follows from (3) that the diode reverse-bias saturation current i_s can be expressed by the open-circuit voltage $v_{oc} = v_{pv}(i_{pv} = 0)$:

$$i_s = \frac{i_{ph} - \frac{v_{oc}}{R_h}}{\exp \left(\frac{1}{A_n} \frac{v_{oc}}{v_T} \right) - 1}. \quad (4)$$

The model parameters A_n and R_h are assumed to be constant. After this, the dependencies from the irradiance and the cell temperature of the variables i_{ph} and v_{oc} , are addressed.

2.2 Array of Photo Cells

Multiple identical photocells are connected in parallel and series to form one PV array. The number of N_p parallel branches multiply with the photo current of one cell and the number of photocells within one branch N_s multiplies with the voltage of one cell. This gives the accumulated current I_{pv} and voltage V_{pv} : $I_{pv} = N_p i_{pv}$, $V_{pv} = N_s v_{pv}$, see Figure 3. Nevertheless, we use the lower case letters in the following to refer to the PV array values, regardless of the number of PV cells used.

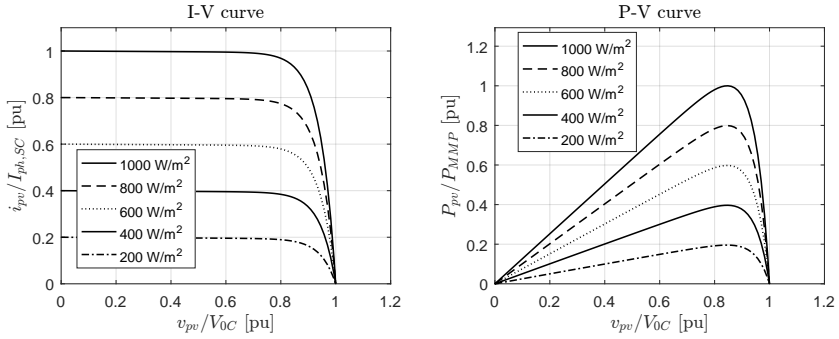


Figure 4: I - V -characteristic (left hand side) and P - V -characteristic (right hand side) for different irradiance.

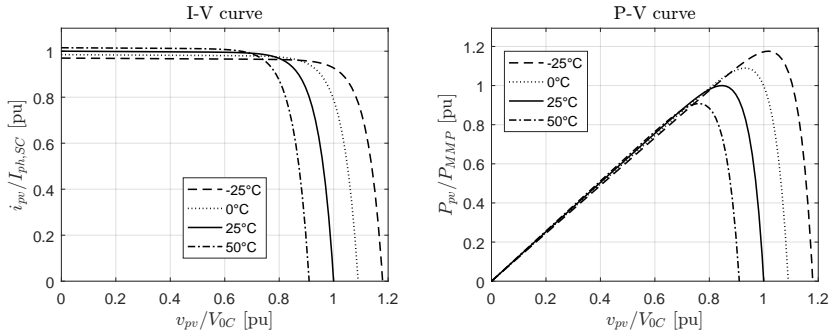


Figure 5: I - V -characteristic (left hand side) and P - V -characteristic (right hand side) for different cell temperatures.

2.3 Variation with Irradiance and Temperature

Derivations from the STC are addressed by the following correction formulas:

$$\frac{i_{ph}}{i_{ph}^{STC}} = \frac{S}{S^{STC}} [1 + \alpha_T (T_c - T_c^{STC})], \quad \frac{v_{oc}}{v_{oc}^{STC}} = 1 + \beta_T (T_c - T_c^{STC}). \quad (5)$$

In the latter formula, the weak impact on the open-circuit voltage by the change of radiation is neglected. The temperature coefficients α_T and β_T are usually given by the manufacturer. One can see the resulting characteristics for change of irradiance and cell temperature in Figure 4 and Figure 5 respectively.

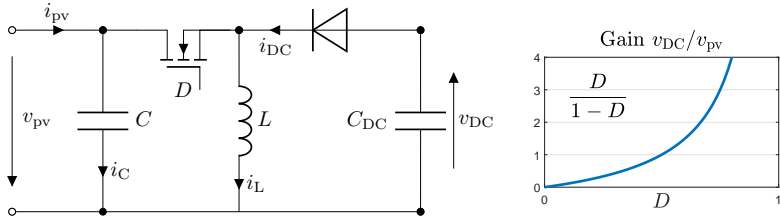


Figure 6: Buck-Boost converter. In switching mode D denotes whether the MOSFET is open ($D = 0$) or closed ($D = 1$). The average value of duty cycle and the corresponding voltage ratio is given in the formula on the right hand side. Consider the definition of v_{DC} in such a way, that v_{DC} has the same sign as v_{pv} .

3 DCDC-Converter

As one can see in (3), the PV cells operating point is controlled via the PV voltage v_{pv} . This voltage is kept constant by a DCDC-Converter which feeds the generated power into a DC link, see Figure 1. Therefore, the converter has to cancel out the disturbances of changing direct link voltage v_{DC} or changes of the incoming PV current i_{pv} .

3.1 Converter Model

We perform our analysis exemplary for three different converters: the buck converter, the boost converter and the buck-boost converter. Circuits and basic equations for these converters can be found in [10], for instance the circuit of the buck-boost converter is given in Figure 6. The converter circuits can be analyzed either for the switch FET (pulse width modulation mode) or as an averaging model. In the first case, D can be either 0 or 1, representing the state of the either closed or opened FET. In the later case $D \in [0, 1]$ represents the average over time of open state of the FET, so called duty cycle D . We define the input and output voltage of the converters in such a way, that they are equal in sign (see Figure 6). Then, the averaging models have the following voltage ratios: $v_{DC}/v_{pv} = D$ (buck converter), $v_{DC}/v_{pv} = 1/(1 - D)$ (the boost converter) and $v_{DC}/v_{pv} = D/(1 - D)$ (buck-boost converter).

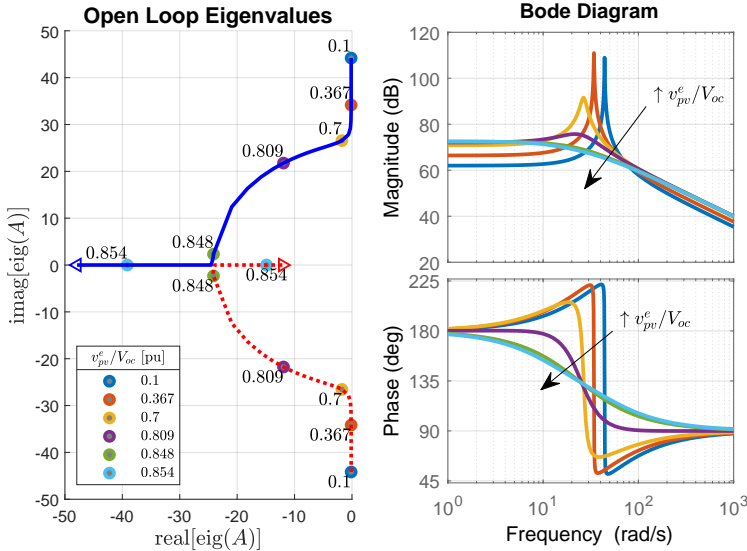


Figure 7: Eigenvalue and Bode diagram for the buck-boost converter coupled with the eSDM.

3.2 Dimensioning of the Electronic parts

The parts used in the converter, namely L and C , are dimensioned in dependence of the nominal operating point. This point is characterized by the maximum power point (MPP) under standard test conditions, i.e. (v_{pv}^0, i_{pv}^0) . On the other side of the converter the nominal direct current link voltage v_{DC}^0 gives the nominal duty cycle D^0 . Finally the pick-to-pick value of ripple current Δi_L and the pick-to-pick value of ripple voltage Δv_{pv} together with the switching frequency f_{sw} are considered:

$$L = \frac{1}{\Delta i_L f_{sw}} \begin{cases} v_{DC}^0(1-D^0) \\ v_{pv}^0 D^0 \\ v_{pv}^0 D^0 \end{cases} \quad C = \frac{1}{\Delta v_{pv} f_{sw}} \begin{cases} i_{pv}^0(1-D^0) & \text{Buck} \\ \Delta i_L/8 & \text{Boost} \\ i_{pv}^0(1-D^0) & \text{Buck-Boost} \end{cases} \quad (6)$$

3.3 State Space Equation and Linearization

Under the assumption, that the polarity of the switch current or voltage does not change during the whole cycle (continuous conduction mode, see [11]), switching mode and average analysis results in the same describing state space equations for the converter:

$$\frac{dv_{pv}}{dt} = \frac{1}{C} \begin{cases} i_{pv} - i_L D \\ i_{pv} - i_L \\ i_{pv} - i_L D \end{cases} \quad \frac{di_L}{dt} = \frac{1}{L} \begin{cases} v_{pv} D - v_{DC} & \text{Buck} \\ v_{pv} - v_{DC}(1-D) & \text{Boost} \\ v_{pv} D - v_{DC}(1-D) & \text{Buck-Boost} \end{cases} \quad (7)$$

Define the input as $u = D$, the states as $\mathbf{x} = (v_{pv}, i_L)^T$ and the function $i_{pv} = f(v_{pv})$ one gets

$$\frac{dx_1}{dt} = \frac{1}{C} \begin{cases} f(x_1) - x_2 u \\ f(x_1) - x_2 \\ f(x_1) - x_2 u \end{cases} \quad \frac{dx_2}{dt} = \frac{1}{L} \begin{cases} x_1 u - v_{DC} & \text{Buck} \\ x_1 - v_{DC}(1-u) & \text{Boost} \\ x_1 u - v_{DC}(1-u) & \text{Buck-Boost} \end{cases} \quad (8)$$

Taylor linearization around one arbitrary stationary operating point (superscript e) defined by $\underline{x}^e = (v_{pv}^e, i_L^e)^T$ and $u^e = D^e$ gives the linear system ($\Delta \underline{x} = \underline{x} - \underline{x}^e$, $\Delta u = u - u^e$)

$$\frac{d}{dt} \Delta \underline{x} = \begin{bmatrix} f'(v_{pv}^e)/C & -a^e/C \\ a^e/L & 0 \end{bmatrix} \Delta \underline{x} + \begin{bmatrix} -b_1^e/C \\ +b_2^e/L \end{bmatrix} \Delta u = \mathbf{A} \Delta \underline{x} + \mathbf{B} \Delta u, \quad (9)$$

$$a^e = \begin{cases} D^e \\ 1 \\ D^e \end{cases} \quad b_1^e = \begin{cases} i_L^e \\ 0 \\ i_L^e \end{cases} \quad b_2^e = \begin{cases} v_{pv}^e & \text{Buck} \\ v_{DC}^e & \text{Boost} \\ v_{DC}^e + v_{pv}^e & \text{Buck-Boost} \end{cases} \quad (10)$$

For all converters $y = v_{pv} = x_1$ applies, and therefore $\Delta y = \mathbf{C} \Delta \underline{x}$, $\mathbf{C} = (1, 0)$.

A brief analysis of the obtained linear models shows a strong dependency of the model properties from the chosen operating point. Assume standard test conditions for temperature and irradiation, then the eigenvalues and bode plots shown in Figure 7 are obtained for different PV voltages v_{pv}^e .

3.4 DCDC-Converter Control Loop

To meet the predefined reference PV voltage $v_{pv,ref}$ a I-state-space controller is used:

$$\Delta D = \Delta u = -\mathbf{K}_x \Delta \mathbf{x} - K_I \int_0^t (v_{pv,ref} - v_{pv}) d\tau. \quad (11)$$

The integral on the right-hand side of (11) can be understood as an additional state. Let be $x_I = \int (v_{pv}^e - v_{pv}) d\tau$ and $x_I^e = \int (v_{pv}^e - v_{pv,ref}) d\tau$, then $\Delta x_I = x_I - x_I^e$ and $\Delta \dot{x}_I = -\mathbf{C} \Delta \mathbf{x}$, under the assumption $v_{pv,ref} = \text{const}$. Collecting the states as one vector this gives the new state space equation:

$$\frac{d}{dt} \Delta \tilde{\mathbf{x}} = \begin{pmatrix} \mathbf{A} & \mathbf{0}_{2 \times 1} \\ -\mathbf{C} & 0 \end{pmatrix} \Delta \tilde{\mathbf{x}} + \begin{pmatrix} \mathbf{B} \\ 0 \end{pmatrix} \Delta u = \tilde{\mathbf{A}} \Delta \tilde{\mathbf{x}} + \tilde{\mathbf{B}} \Delta u, \quad \Delta \tilde{\mathbf{x}} = \begin{pmatrix} \mathbf{x} - \mathbf{x}^e \\ x_I - x_I^e \end{pmatrix}. \quad (12)$$

Following this scheme, the controller can be written as state space controller, namely $\Delta u = -\tilde{\mathbf{K}} \Delta \tilde{\mathbf{x}}$ and $\tilde{\mathbf{K}} = (\mathbf{K}_x^T, K_I)^T$.

3.5 LMI Controller Design - Single Model

The controller in form of the matrix $\tilde{\mathbf{K}}$ can be found using linear matrix inequalities (LMIs) conditions. The conditions are in general derived from analysis using the Direct method of Lyapunov [12]. A common Lyapunov function candidate is of the quadratic form, $V = \mathbf{x}^T \mathbf{P} \mathbf{x}$. Together with the controller and the state space equation this gives the matrix inequality that contains the unknown controller $\tilde{\mathbf{K}}$ and the variable \mathbf{P} :

$$\forall \mathbf{x}: \frac{dV}{dt} = \frac{d}{dt} (\mathbf{x}^T \mathbf{P} \mathbf{x}) = \mathbf{x}^T \underbrace{[(\tilde{\mathbf{A}} - \tilde{\mathbf{B}} \tilde{\mathbf{K}})^T \mathbf{P} + \mathbf{P}(\tilde{\mathbf{A}} - \tilde{\mathbf{B}} \tilde{\mathbf{K}})]}_{<0} \mathbf{x} < 0. \quad (13)$$

Their feasibility can be verified by finding a solution using interior-point methods [13]. In this study we use the Yalmip library for Matlab [14] together with the Mosek solver [15].

The inequation (13) can be extended to add some restrictions about the closed-loop pole [16]. In this, we set a minimum decay rate α , a minimum damping

Table 1: Parameter of the single model

parameter	$v_{pv}^e/v_{pv,MPP}$	$S^e = S^{STC}$	$T_c^e = T_c^{STC}$	α	Θ	r
value	0.9	1000 W/m ²	298 K	25	20°	51

ratio $\zeta = \cos(\Theta)$, and a maximum undamped natural frequency $\omega_d = r \sin(\Theta)$. The so defined area and the actual area of the poles are marked in Figure 8a.

For the single model, containing only one operational point, the restrictions are given in Table 1. The so found controller has the closed-loop eigenvalues shown in Figure 8a. While the behavior of this controller around its operational point is quite satisfactory, larger deviations from this operational point give poor results in terms of overshoot and oscillations, see Figure 8b. Therefore the Takagi-Sugeno Model will be used in the next steps, utilizing multiple operation points.

3.6 Takagi-Sugeno (TS)-Model

The nonlinear system under investigation is described via the equations:

$$\dot{\mathbf{x}} = \mathbf{f}(\mathbf{x}, \mathbf{u}, \boldsymbol{\theta}), \quad \mathbf{x}_0 = \mathbf{x}(t_0), \quad \mathbf{y} = \mathbf{g}(\mathbf{x}), \quad (14)$$

where

$$\left\{ \begin{array}{ll} \mathbf{f}: \mathbb{R}^n \rightarrow \mathbb{R}^n, & \text{smooth vector-valued function} \\ \mathbf{g}: \mathbb{R}^n \rightarrow \mathbb{R}^p, & \text{smooth vector-valued function} \\ \mathbf{x} \in \mathbb{R}^n, & \text{state space vector} \\ \mathbf{u} \in \mathbb{R}^m, & \text{input vector with controllable and uncontrollable inputs} \\ \mathbf{y} \in \mathbb{R}^p, & \text{output vector} \\ \boldsymbol{\theta} \in \mathbb{R}^d, & \text{time variable parameter vector} \end{array} \right.$$

Taylor linearization of (14) around $i = 1, 2, \dots, N_r$ different equilibrium points $\{\mathbf{x}_i^e, \mathbf{u}_i^e\}$ which fulfill $\mathbf{f}(\mathbf{x}_i^e, \mathbf{u}_i^e) = \mathbf{0}$ gives

$$\Delta \dot{\mathbf{x}}_i = \mathbf{A}_i \Delta \mathbf{x}_i + \mathbf{B}_i \Delta \mathbf{u}_i, \quad \Delta \mathbf{y}_i = \mathbf{C}_i \Delta \mathbf{x}_i. \quad (15)$$

All these linear systems share the same state and input vector. The TS model is the weighted sum of these linear systems, giving an interpolation of N_r LTI systems:

$$\dot{\mathbf{x}} = \sum_{i=1}^{N_r} h_i(\underline{\mathbf{z}}) (\mathbf{A}_i \mathbf{x} + \mathbf{B}_i \mathbf{u} + \mathbf{a}_i), \quad \mathbf{a}_i = -\mathbf{A}_i \mathbf{x}_i^e - \mathbf{B}_i \mathbf{u}_i^e \quad (16)$$

$$\mathbf{y} = \sum_{i=1}^{N_r} h_i(\underline{\mathbf{z}}) (\mathbf{C}_i \mathbf{x} + \mathbf{c}_i), \quad \mathbf{c}_i = -\mathbf{C}_i \mathbf{x}_i^e \quad (17)$$

The functions $h_i : \mathbb{R}^l \rightarrow \mathbb{R}$ are the membership functions and fulfill the convex sum condition: $\forall \mathbf{z} : \sum h_i(\mathbf{z}) = 1$. The vector of the so-called premise variables \mathbf{z} may directly contains states x_k , inputs u_k , and time variable parameters θ_k or be a function $\mathbf{z} = \mathbf{z}(\mathbf{x}, \mathbf{u}, \theta)$. In the following we assume, that the equilibrium points are selected by premise variables \mathbf{z}^e , arranged on a Cartesian grid. Then we can switch from one linear index i (numbering all models from 1 to N_r) to a total of d Cartesian coordinates i_1, i_2, \dots, i_d (number of premise variables is equal to d). The transformation between both ways of indexing is given by:

$$\mathbf{z}_i^e = [z_{1,i_1}^e, z_{2,i_2}^e, \dots, z_{d,i_d}^e]^T, \quad \begin{cases} i_k = 1 \dots n_k \\ k = 1 \dots d \end{cases} \Rightarrow i = 1 + \sum_{k=1}^d (i_k - 1) \prod_{l=1}^{k-1} n_l. \quad (18)$$

The membership functions are constructed as products of local test-functions

$$h_i(\mathbf{z}) = h_{i_1, i_2, \dots, i_d}(\mathbf{z}) = \prod_{k=1}^d w_{k, i_k}(z_k), \quad \mathbf{z} = [z_1, z_2, \dots, z_d]^T. \quad (19)$$

These local test-functions are almost everywhere zero, equals one only at the corresponding supporting point, that is $w_{k, i_k}(z_{k, j_k}^e) = \delta_{i_k, j_k}$ (δ_{ij} is the Kronecker delta), and are interpolated by a given function g between.

Table 2: Parameter defining the operational points of the TS-Model

parameter	values
$v_{pv,i}^e / v_{pv,MPP}$	$\{0.3, 0.6, 0.9\}$
S_i^e	$\{200, 333, 467, 600, 733, 867, 1000\} \text{ W/m}^2$
$T_{c,i}^e$	$\{273, 303, 333\} \text{ K}$

Assuming ascending order of the supporting points, $z_{k,j_k-1}^e < z_{k,j_k}^e$, this can be written as

$$w_{k,i_k}(z_k) = \begin{cases} 1 & , z_k \leq z_{k,1}^e \text{ or } z_{k,n_k}^e \leq z_k \\ g \left(\frac{|z_k - \hat{z}_{k,i_k}|}{|z_{k,i_k}^e - z_{k,i_k-1}^e|} \right) & , z_{k,i_k-1}^e \leq z_k \leq z_{k,i_k}^e \\ g \left(\frac{|z_k - z_{k,i_k}^e|}{|z_{k,i_k}^e - z_{k,i_k+1}^e|} \right) & , z_{k,i_k}^e \leq z_k \leq z_{k,i_k+1}^e \\ 0 & , \text{otherwise} \end{cases} \quad (20)$$

In this we use a very simple function g that satisfy the convex sum condition, namely $g(x) = 1 - x$, which gives triangular shaped test-functions.

Under stationary conditions three parameters are needed to determine the state of the systems, they form the vector of premise variables $\mathbf{z} = (v_{pv}, S, T_c)^T$. The parameters defining the chosen 63 models, are given in Table 2.

3.7 LMI Controller Design - TS-Model

The TS-Model is now used to find controller for each operational point, in such a way that the following control law is applicable:

$$u = D = \sum_{i=1}^{N_f} h_i [D_i^e - \mathbf{K}_{x,i}(\mathbf{x} - \mathbf{x}_i^e) - K_{I,i}x_I], \quad x_I = \int_0^t (v_{pv,\text{ref}} - v_{pv}) d\tau. \quad (21)$$

The methodology in applying the Direct method of Lyapunov is the same as before. But now, multiple inequations of the type (13) has to be solved simultaneously for different matrices $\tilde{\mathbf{K}}_i$ but the same variable \mathbf{P} . Using the same \mathbf{P} guarantee not only local stability, but global stability. Like before,

additional constraints are applied to the LMIs. They are chosen independently for each model:

$$\alpha_i = 2 \times \lambda_{\min, \text{Re}, i}^{\text{open-loop}}, \quad r_i = 10 \times \lambda_{\max, \text{Abs}, i}^{\text{open-loop}}, \quad \Theta = 20^\circ \quad (22)$$

with

$$\begin{cases} \lambda_{\min, \text{Re}, i}^{\text{open-loop}}, & \text{smallest absolute real part of the open-loop eigenvalues} \\ \lambda_{\max, \text{Abs}, i}^{\text{open-loop}}, & \text{largest norm of the open-loop eigenvalues} \end{cases}$$

The position of the eigenvalues is exemplary given for two models in Figure 8a. The simulation results shows a much better performance for the TS-controller than for the single controller, see Figure 8c.

4 MPP and DPP Tracking Methods

Classical MPP techniques can be divided into offline techniques, like the fractional open-circuit voltage and the fractional short-circuit current techniques; online techniques, like the perturb-and-observe and the incremental conductance techniques; and advanced (by means of computational effort) techniques [17].

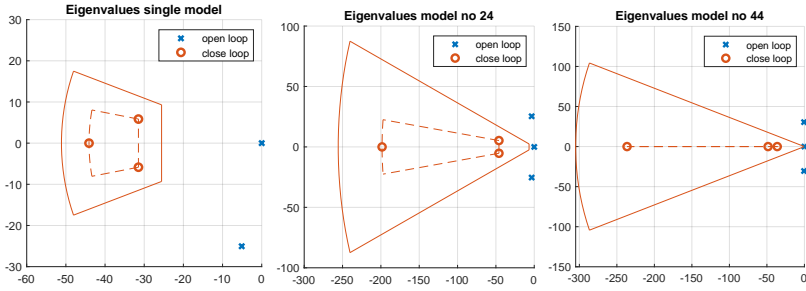
In this we use the perturb and observe (P&O) method, e.g. [18, 19, 20], and extend this method for DPP tracking. The basic idea of this method is to vary (perturb) the PV voltage and to observe the change in the power output. The direction of the voltage steps is kept if the power increases and reverses otherwise. Metaphorically speaking, the operational point moves towards the extremum, hence this method is also called hill climbing method. Once it reached the MPP, the system will oscillate about the MPP. Choice of the step size affects both, the time it takes to reach the MPP and the minimal distance to the MPP due to the oscillations. The first effect makes a large as reasonable step size desirable, the second effect forces the step size to be as small as possible.

The perturb and observe method can fail under changing irradiation conditions. If irradiation increases, then regardless of the direction of the perturbation, the power output is increasing and the algorithm will keep the direction. In [21] a three-point weight comparison P&O method is used to overcome this problem.

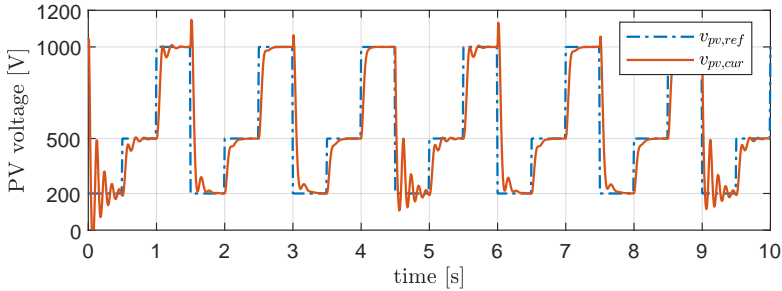
Extension for DPP tracking can be done by replacing the feedback from the produced power $P_{pv} = v_{pv} \times i_{pv}$ to the function $P_{pv}^* = -|P_{pv} - P_{dem}|$. One can see, that this results in a large range for the PV voltage, which makes the advanced TS controller useful if not necessary.

5 Conclusion

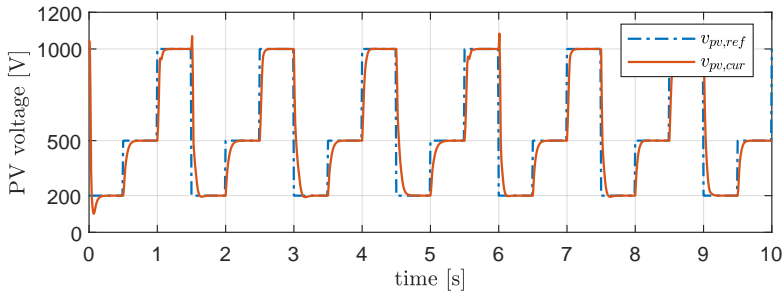
The modelling of a PV power station has been described. Power conversion is performed within two steps, firstly by a buck-boost converter adjusting the power to the DC link level, secondly by an inverter meeting the requirements of the point of common coupling. The first conversion step is described in detail since here a modified Perturb and Observation method is applied to realise a DPP tracking. To cover a large operation range of the converter, the PV voltage solely adjusts the PV current and therefore the produced power, a Takagi-Sugeno Modell is used. The improved performance of the multi-operational point model has been shown in the simulation. This paper shows one way, how PV plants can contribute more to grid stability. An inevitable feature on the market of growing PV power share.



- (a) Shown are the Eigenvalues of the open-loop and closed-loop models. The single model (left-hand side) arises from the linearization at one operational point only. On the contrary, the TS model arises from 63 different operational points. Eigenvalues for the TS model number 24 (middle) and 44 (right-hand side) are shown.



- (b) Shown is the step response in the PV voltage $v_{pv,cur}$ for the single model (controller design for one operational point). The values of the reference PV voltage $v_{pv,ref}$, irradiation S , and cell temperature T_c change their values abruptly every 0.5 seconds.



- (c) Shown is the step response in the PV voltage $v_{pv,cur}$ for the TS model (controller design for a total of 63 operational points). The values of the reference PV voltage $v_{pv,ref}$, irradiation S , and cell temperature T_c change their values abruptly every 0.5 seconds.

References

- [1] B. Kroposki, B. Johnson, Y. Zhang, V. Gevorgian, P. Denholm, B.-M. Hodge, and B. Hannegan, “Achieving a 100% Renewable Grid: Operating Electric Power Systems with Extremely High Levels of Variable Renewable Energy,” *IEEE Power and Energy Magazine*, vol. 15, pp. 61–73, Mar. 2017.
- [2] T. Esram and P. Chapman, “Comparison of Photovoltaic Array Maximum Power Point Tracking Techniques,” *Energy Conversion, IEEE Transactions on*, vol. 22, pp. 439–449, July 2007.
- [3] F. Pöschke, E. Gauterin, M. Kühn, J. Fortmann, and H. Schulte, “Load mitigation and power tracking capability for wind turbines using linear matrix inequality-based control design,” *Wind Energy*, vol. 23, no. 9, pp. 1792–1809, 2020.
- [4] W. W. Simon Philipps, “Photovoltaics report,” tech. rep., Fraunhofer ISE, PSE Projects GmbH, Sept. 2020.
- [5] N. Klaes, N. Goldschmidt, and J. Fortmann, “Voltage Fed Control of Distributed Power Generation Inverters with Inherent Service to Grid Stability,” *Energies*, vol. 13, p. 2579, Jan. 2020.
- [6] S. D’Arco and J. A. Suul, “Equivalence of Virtual Synchronous Machines and Frequency-Droops for Converter-Based MicroGrids,” *IEEE Transactions on Smart Grid*, vol. 5, pp. 394–395, Jan. 2014.
- [7] B. Marinescu, O. Gomis-Bellmunt, F. Dörfler, H. Schulte, and L. Sigrist, “Dynamic Virtual Power Plant: A New Concept for Grid Integration of Renewable Energy Sources,” *arXiv:2108.00153 [cs, eess]*, July 2021. arXiv: 2108.00153.
- [8] W. Xiao, *Photovoltaic Power System: Modeling, Design, and Control*. Wiley, 2017.
- [9] W. Shockley, “The theory of p-n junctions in semiconductors and p-n junction transistors,” *The Bell System Technical Journal*, vol. 28, no. 3, pp. 435–489, 1949.

- [10] R. W. Erickson, "DC–DC Power Converters," in *Wiley Encyclopedia of Electrical and Electronics Engineering*, American Cancer Society, 2007.
- [11] R. W. Erickson and D. Maksimovic, *Fundamentals of Power Electronics*. Springer US, 2 ed., 2001.
- [12] A. M. LYAPUNOV, "The general problem of the stability of motion," *International Journal of Control*, vol. 55, pp. 531–534, Mar. 1992.
- [13] Y. Nesterov and A. Nemirovskii, *Interior-Point Polynomial Algorithms in Convex Programming*. Studies in Applied and Numerical Mathematics, Society for Industrial and Applied Mathematics, Jan. 1994.
- [14] J. Löfberg, "Yalmip : A toolbox for modeling and optimization in matlab," in *In Proceedings of the CACSD Conference*, (Taipei, Taiwan), 2004.
- [15] MOSEK ApS, *The MOSEK optimization toolbox for MATLAB manual. Version 9.0.*, 2019.
- [16] M. Chilali and P. Gahinet, " H_∞ design with pole placement constraints: an LMI approach," *IEEE Transactions on Automatic Control*, vol. 41, pp. 358–367, Mar. 1996.
- [17] A. Eltamaly and A. Abdelaziz, *Modern Maximum Power Point Tracking Techniques for Photovoltaic Energy System*. Aug. 2019.
- [18] O. Wasynczuk, "Dynamic Behavior of a Class of Photovoltaic Power Systems," *IEEE Transactions on Power Apparatus and Systems*, vol. PAS-102, pp. 3031–3037, Sept. 1983.
- [19] W. Teulings, J. Marpinard, A. Capel, and D. O’Sullivan, "A new maximum power point tracking system," in *Proceedings of IEEE Power Electronics Specialist Conference - PESC '93*, pp. 833–838, June 1993.
- [20] N. D’Souza, L. Lopes, and X. Liu, "An Intelligent Maximum Power Point Tracker Using Peak Current Control," in *2005 IEEE 36th Power Electronics Specialists Conference*, pp. 172–, June 2005. ISSN: 2377-6617.

- [21] Y.-T. Hsiao and C.-H. Chen, “Maximum power tracking for photovoltaic power system,” in *Conference Record of the 2002 IEEE Industry Applications Conference. 37th IAS Annual Meeting (Cat. No.02CH37344)*, vol. 2, pp. 1035–1040 vol.2, Oct. 2002. ISSN: 0197-2618.